AUTOMATIC QUANTIFICATION OF THREE-DIMENSIONAL VELOCITY FIELD IMPROVED BY SPATIALLY VARYING AVERAGING FILTERS

J. A. Sims *, S. S. Furuie**, M. A. Gutierrez *

*Department of Informatics, Heart Institute (InCor),
São Paulo, Brazil
**School of Engineering, University of São Paulo,
São Paulo, Brazil

e-mail: John.sims@incor.usp.br

Abstract: *Automatic methods for quantifying velocity in cardiac images can be used to diagnose diseases, but the estimated velocity suffers from blurring in the region of motion discontinuities when using variational methods. In this paper, spatially varying filters were used to improve accuracy in these regions. These filters depend on: (i) image intensity and (ii) velocity estimates from previous iterations of the update equation. Methods were extended to voxel space, tested with synthetic images, and parameters optimized. The spatially varying filter which depends on velocity estimates was found to provide the greatest reduction in error measures, but the benefits were found to depend on careful choices of derivative scheme and other model parameters.*

Keywords: *Optical flow, automatic quantification, left-ventricular motion, spatially varying averaging filters*

Introduction

Cardiac pathologies, such as Ventricular Dyssynchrony, Ischemia or Noncompaction Cardiomyopathy, can produce changes in the normal motion of the left ventricle. Accurate quantification of movement can therefore assist in the diagnosis of these pathologies. Automatic methods for quantification are used due to the complexity and size of the images, objectivity, speed, and cost considerations. The variational Optical Flow (OF) technique proposed by Horn and Schunck [1], extended to voxel space, is a possible method for motion quantification, whereby the true motion field is estimated from a sequence of three-dimensional images (4D, meaning 3D plus time). Although the method is fast and simple, inaccuracies in velocity estimation are exaggerated at motion boundaries, the surfaces between neighbouring volumes where discontinuities in regional velocity are encountered.

Gauss-Seidel (GS) update equations can be used for iterative solution of the OF linear equations to produce the velocity field [1]. These equations, extended to voxel space, have the form shown in equation (1). [2] shows equations for the three velocity components, but for brevity only the x component of velocity is shown:

$$u^{k+1} = \overline{u}^{k} - \frac{E_x(E_x\overline{u}^{k}+E_y\overline{v}^{k}+E_z\overline{w}^{k}+E_t)}{\alpha^2+E_x^2+E_y^2+E_z^2} \qquad (1)$$

where k is the iteration index; $\overline{u}, \overline{v}, \overline{w}$ are mean velocities in x, y, z; E_x, E_y, E_z are partial derivatives of image intensity E(x,y,z,t) and α^2 is a regularization parameter. In Horn and Schunck's paper [1] the mean velocities are calculated using a set of fixed filter coefficients, which mixes velocity values when applied to motion boundary pixels (Non-Adaptive Method, NAM). An alternative is to use Spatially Varying Filters (SVFs), where the pixels used to calculate mean values are selected according to: (i) intensity values of the image using an Adaptive Intensity Method (AIM); (ii) evolving velocity characteristics using an Adaptive Velocity Method, (AVM) [3].

The objectives of this paper are to investigate and quantify possible improvements in OF accuracy in 4D images when using SVFs (AIM and AVM), compared to a fixed weight averaging filter (NAM), and to determine the conditions under which improvements are maximised. For this preliminary study, textured cylinders in rotation and translation were used, but our future aim is to study these improvements using XCAT phantom data [4]. XCAT is a 4D extended cardiac-torso phantom, able to produce realistic imaging data. It also produces frame-by-frame voxel positions, from which Ground Truth (GT) velocity estimates can be obtained. These are expected values of velocity, from which error in the OF can be calculated.

Materials and methods

An extension of the Horn and Schunck algorithm to voxel space was developed in MATLAB 2013a. The model was changed to accommodate the following schemes for derivatives and mean velocities.

Schemes for estimating derivatives – two schemes using kernel convolution were implemented: i. Simple Kernel (SK), [-1, 0, 1] in x, y, z, and t; ii. Simoncelli's Matched/ Balanced kernels (MB) [2]. Volumes were padded with mirrored values before convolution.

Schemes for calculating mean velocity - three schemes were implemented:

1. NAM provides a baseline comparison for the adaptive algorithms, and uses convolution with a fixed kernel to provide a weighted average over the 18 neighbourhood:

$$\bar{u}_{i,j,k} = \frac{1}{9}\left(u_{i+1,j,k} + u_{i-1,j,k} + u_{i,j+1,k} + u_{i,j-1,k} + u_{i,j,k+1} + u_{i,j,k-1}\right) + \frac{1}{36}\left(u_{i+1,j+1,k} + u_{i-1,j+1,k} + u_{i+1,j-1,k} + u_{i-1,j-1,k} + u_{i+1,j,k+1} + u_{i+1,j,k-1} + u_{i-1,j,k+1} + u_{i-1,j,k-1} + u_{i,j+1,k+1} + u_{i,j-1,k+1} + u_{i,j+1,k-1} + u_{i,j-1,k-1}\right) \quad (2)$$

where i,j,k are the coordinates of the central voxel.

2. AIM uses formulae extended to 3D sequences from [5], with values calculated over the 26 neighbourhood. The smoothing filter, ϕ_I, calculates $\bar{u}, \bar{v}, \bar{w}$ depending on the intensity difference between the central voxel, i, and each of the 26 neighbours ($j \in N_i$).

$$\phi_I = \sum_{j \in N_i} \gamma_j \mu_j \quad (3)$$

where γ_j represents the contribution of a voxel, j, in the neighbourhood of central voxel i, and μ_j represents one of the velocities u_j, v_j, w_j, which is being averaged. The normalized value of γ_j for a neighbouring voxel is calculated using equation (4), where I_i is the intensity of the central voxel and I_j the intensity of the jth voxel.

$$\gamma_j = \frac{\frac{1}{1+|I_j - I_i|}}{\sum_{j=1}^{26} \frac{1}{1+|I_j - I_i|}} \quad (4)$$

3. AVM was extended to voxel space from [5]. The filter has the same form as equation (3) with filter coefficients calculated using equation (5):

$$\gamma_j = \frac{\left(1+\left|\mu_j - \mu_i\right|\right)^{-\beta}}{\sum_{j=1}^{26}\left(1+\left|\mu_j - \mu_i\right|\right)^{-\beta}} \quad (5)$$

where β>1, and μ_i and μ_j represent one of the velocities u, v, or w. β accounts for possible small differences in the velocity values [3], and optimum values of β were found empirically. Three values of β were tested, referred to as AVM5, AVM6, AVM7, where β takes the value of 5, 6, 7 respectively.

Generation of synthetic images and corresponding ground truth velocities - Synthetic image sequences of a textured cylinder in rotation and translation were generated against a non-textured background [6]. The constant term for the texture was 0.5 and the amplitude for the sinusoids was 0.25, creating a texture varying between zero and one. The image background was set to zero. Total image dimensions were 74 by 74 by 5 (x, y, z), with a cylinder of radius 28 and height 5 voxels. Figure 1 shows a volume rendering of a single frame.

Five image sequences for the cylinders were used as shown in Table 1. Frames 1 to 5 were used for the MB scheme and frames 2 to 4 for SK, the result being calculated only at frame 3. For each image sequence, a total of 120 tests were performed, permutations of 5 averaging methods (NAM, AIM, AVM5, AVM6, AVM7), 2 methods for calculating derivatives (SK and MB), 3 values of iteration (50,100,150) and 4 values of α^2 (0.2, 0.5, 1.0 and 1.5), producing a total of 600 tests. GT velocities were generated for each image.

Table 1: Image sequences used in the tests.

Sequence 1	rotation of 1 degree per frame
Sequence 2	rotation of 2 degrees per frame
Sequence 3	rotation of 5 degrees per frame
Sequence 4	translation of (u,v,w) = (1, 0, 0)
Sequence 5	translation of (u,v,w) = (1, 1, 0)

where u, v, and w are velocities in x, y, z directions.

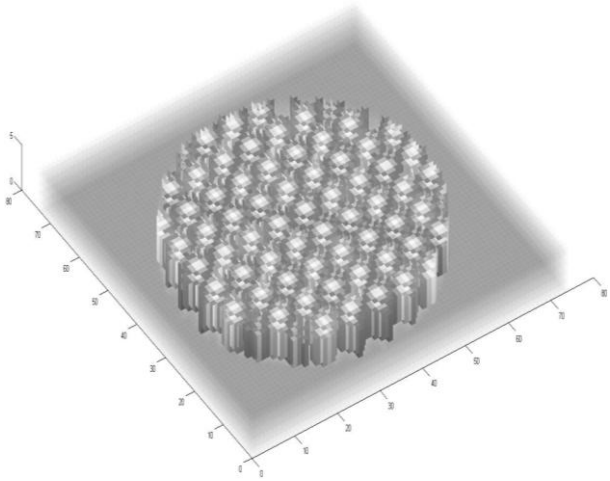

Figure 1: Single frame of the cylinder used in the tests.

Error measures were defined to quantify differences between method and GT velocities. Root Mean Square Error (RMSE) and Normalized RMSE (NRMSE) were calculated according to equations (6) and (7):

$$RMSE = \sqrt{\frac{\sum_{i,j,k=1}^{I,J,K}[\epsilon_u(i,j,k)^2 + \epsilon_v(i,j,k)^2 + \epsilon_w(i,j,k)^2]}{IJK}} \quad (6)$$

$$NRMSE = 100\sqrt{\frac{\sum_{i,j,k=1}^{I,J,K}[\epsilon_u(i,j,k)^2 + \epsilon_v(i,j,k)^2 + \epsilon_w(i,j,k)^2]}{\sum_{i,j,k=1}^{I,J,K}\left[\{u_{gt}(i,j,k)\}^2 + \{v_{gt}(i,j,k)\}^2 + \{w_{gt}(i,j,k)\}^2\right]}} \quad (7)$$

where the image is of dimensions I by J by K voxels, i, j, k, are velocity vector coordinates in voxel space, u_{GT}, v_{GT}, w_{GT} GT velocities, ϵ_u, ϵ_v and ϵ_w are errors between method and ground truth velocities.

End-Point Error (EE) and Angular Error (AE) were calculated according to equations (8) and (9), then Average EE and AE (AEE and AAE) calculated both globally and Within Volume (WV), meaning inside the cylinder volume.

$$\text{EE} = \sqrt{(u - u_{GT})^2 + (v - v_{GT})^2 + (w - w_{GT})^2} \quad (8)$$

$$\text{AE} = \cos^{-1}\left(\frac{u.u_{GT} + v.v_{GT} + w.w_{GT}}{\sqrt{u_{GT}^2 + v_{GT}^2 + w_{GT}^2}\sqrt{u^2 + v^2 + w^2}}\right) \quad (9)$$

AE was set to zero if the magnitude of either vector was below the threshold 0.001 to avoid indeterminate values, meaning that all AE values outside the cylinder volume are zero. AAE is therefore not a global measure

in the tests, and while included for completeness, cannot be directly compared with other global errors presented.

Results

All statistics were calculated from raw values of OF, with no post-smoothing applied. In all cases the AVM that minimised NRMSE was selected as the best representative of AVM5, AVM6, AVM7 and presented alongside NAM and AIM.

Table 2 shows results obtained for Sequence 1 using derivative estimation methods SK and MB and averaging methods NAM, AIM and AVM for 50 iterations and optimum α^2.

Table 2 Best results obtained for frame 3 of Sequence 1

		Global		Within volume	
measure	**method**	**SK**	**MB**	**SK**	**MB**
NRMSE (%)	NAM	31.1	32.8	17.4	12.3
	AIM	34.0	36.3	16.5	12.1
	AVM7	28.5	33.0	17.0	12.7
RMSE (voxels)	NAM	0.072	0.075	0.040	0.028
	AIM	0.078	0.084	0.038	0.028
	AVM7	0.065	0.076	0.039	0.029
AEE (voxels)	NAM	0.044	0.041	0.021	0.009
	AIM	0.051	0.049	0.021	0.010
	AVM7	0.043	0.043	0.020	0.010
AAE (°)	NAM	0.0069	0.0058	0.0069	0.0058
	AIM	0.0060	0.0052	0.0060	0.0052
	AVM7	0.0062	0.0056	0.0062	0.0056

For SK, AVM7 provided best global values for NRMSE and RMSE with α^2=0.2 and 50 iterations, AEE with α^2 of 0.5 and 50 iterations and AAE with α^2 1.5 and 150 iteration. For MB, lowest global values of NRMSE, RMSE, AEE were found with the averaging algorithm NAM with α^2=0.2 and 50 iterations, while AIM provided lowest AAE with α^2 =0.2 and 150 iterations. Overall SK produced lower errors than MB.

Figure 2 compares the accuracy of the OF algorithms using two global error measures, NRMSE and AEE for MB derivatives. NAM produced only slight improvement over AVM7 for 50 iterations and α^2=0.2. AIM produced results with the highest error. As α^2 increases, the difference between the methods is less pronounced.

For Sequence 2 lowest global errors were produced by AVM7 for NRMSE, RMSE and AEE with SK and α^2=0.5, and 50 iterations, whereas lowest AAE was produced by AIM with MB, α^2 = 1.5 and 50 iterations.

For Sequence 3, optimum results were found with AVM5 combined with SK as shown in Table 4. The combination minimised NRMSE, RMSE, AEE, AAE to 44.7%, 51.6%, 0.32 voxels and 0.034° respectively.

The optimum combination for Sequence 4 was found with AVM7 and the SK derivative scheme. Table 3 shows the best results obtained.

The optimum combination for Sequence 5 was found with AVM5 and SK derivatives. However, errors for AVM7 were only 2% larger for NRMS and 1.7% smaller for AEE than AVM5.

Discussion

Figure 2 shows that NRMSE is strongly dependent on the value of α^2 for rotation and translation. Lower values of α^2 produce much lower error and, in the case of SK, produce a larger difference between averaging methods. A lower value of α^2 places confidence in the derivatives rather than the smoothness of the OF, which seems reasonable in the situation where flow is discontinuous at the motion boundary.

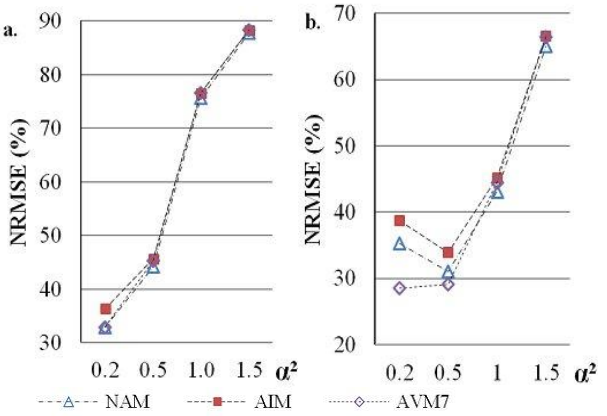

Figure 2: Global NRMSE against α^2 for Sequence 1 with 50 iterations and averaging methods NAM, AIM and AVM7 for (a) MB (b) SK derivatives scheme.

Table 3: Best results obtained for frame 3 of Sequence 4

		Global		Within volume	
measure	**method**	**SK**	**MB**	**SK**	**MB**
NRMSE (%)	NAM	32.3	37.5	1.7	5.6
	AIM	34.3	39.3	1.6	5.2
	AVM7	20.6	33.3	1.8	5.4
RMSE (voxels)	NAM	0.216	0.251	0.011	0.0004
	AIM	0.230	0.263	0.011	0.0004
	AVM7	0.138	0.223	0.012	0.0004
AEE (voxels)	NAM	0.119	0.147	0.0024	0.011
	AIM	0.135	0.158	0.0025	0.011
	AVM7	0.033	0.128	0.0008	0.010
AAE (°)	NAM	0.0013	0.0045	0.0013	0.0045
	AIM	0.0013	0.0042	0.0013	0.0042
	AVM7	0.0003	0.0040	0.0003	0.0040

Table 4: Optimum model combinations by sequence

Image Sequence	Method	NRMSE α^2, iter	RMSE α^2,iter	AEE α^2,iter	Derivative scheme
1	AVM7	0.2, 50	0.2, 50	0.5, 50	SK
2	AVM7	0.5, 50	0.5, 50	0.5, 50	SK
3	AVM5	0.5, 50	0.5, 50	0.5, 50	SK
4	AVM7	0.5, 50	0.5, 50	0.5, 50	SK
5	AVM5	0.5, 100	0.5, 100	0.5, 100	SK

For sequences 1 to 4, NRMSE, RMSE and AEE were minimized with 50 iterations. A larger number of iterations creates increased diffusion of OF across the motion boundary, and OF outside of the volume is heavily penalised by the error measures. For Sequence 5, where optimized errors were generated with 100 iterations, the velocity is larger and perhaps requires more iterations to converge to this larger value of OF.

The choice of derivative scheme was seen to have an effect on the error measures. The global measures show that SVFs offer little or no improvement over NAM when using MB, but when using SK a substantial improvement of accuracy for AVM is obtained. MB provides a larger neighbourhood of points for the derivative estimate, smoothing noise, but the derivative become less representative of local changes. MB would seem to be more appropriate for smoothly changing image regions than close to motion boundaries, where the derivative estimate mixes distinct image regions. Future work might investigate an adaptive algorithm for differentiation, which bases estimates on local image statistics.

Equation (1) shows that a smaller value of α^2 decreases the contribution of the smoothness term to evolving OF. OF can be accurate at the motion boundary only when the average values and derivatives, which constitute the second term, accurately represent this part of the image.

WV results for the MB scheme are consistently better than those of SK for sequence 1; the magnitude of error generated at the motion boundary is larger than that generated within the volume, resulting in superior global performance of the SK derivative scheme.

AIM outperformed AVM or NAM only in Sequence 2, where it produced the lowest AAE value. [5] similarly showed that AIM produced inferior results to AVM, although different error measures were used.

For the sequences studied, optimum combinations were achieved using AVM7, SK derivatives scheme, 50 and 100 iterations and α^2 between 0.2 and 0.5.

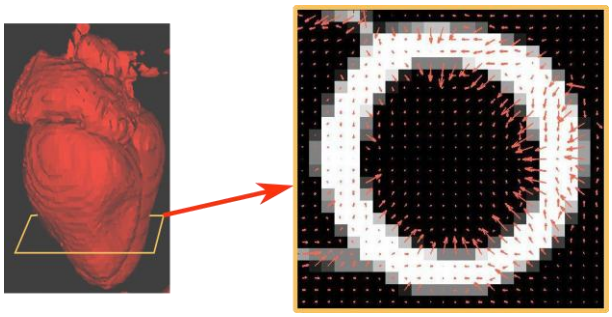

Figure 3: a) 3d rendering of XCAT myocardium showing a representative transaxial slice; b) Transaxial slice of XCAT left ventricle during systole with optical flow superimposed, calculated using AVM7, 50 iterations of algorithm and α^2=0.2.

Limitations of the study – the tests presented used synthetic images, which are similar to cardiac image sequences only in terms of general motion (rotation and translation). Future studies will extend the proposed method to cardiac XCAT images, determining optimum settings for the spatially varying filters and other model parameters. Figure 3a shows a volume from an XCAT sequence and Figure 3b shows OF for a transaxial slice of the XCAT sequence in systole, calculated using the optimal combination of methods and parameters found in this study, SK, AVM7, 50 iterations and α^2=0.2.

Noise was not added to the synthetic images, which limits the importance of any findings, since images in Nuclear Medicine are degraded by noise, in particular of type Poisson. It is possible that the advantages of using SK do not outweigh MB kernels when noise is present in the images.

Contributions of this research to state of the art – This study showed potential benefits of extended SVFs to 4D cardiac sequences through their application to synthetic images with cylinders, and applied statistical analysis to determine the optimum parameters and schemes.

Conclusion

AVM produced the best global results compared to NAM and AIM. Lowest errors were found with a lower number of iterations, low value of α^2 and using SK derivative scheme. However, when AVM is paired with MB derivatives, the improvement disappears. Error increases as α^2 and number of iterations is increased.

Acknowledgements

The authors would like to thank FUSP for their financial support.

References

[1] Horn BKP, Schunck BG. Determining optical flow, Artificial intelligence, 17:185-203, 1981

[2] Barron JL, Thacker NA. Tutorial: Computing 2D and 3D Optical Flow, Tina Memo No. 2004-012, 2005.

[3] Mitiche A, Aggarwal JK. Computer Vision Analysis of Image Motion by Variational Methods, Cham, Springer International Publishing, 2014.p. 41-93

[4] Segars WP, Sturgeon G, Mendonca S, Grimes J, Tsui BMW. 4D XCAT phantom for multimodality imaging research. Med Phys. 37 (9), 4902-4915, September 2010

[5] El-Feghali R, Mitiche A. Fast Computation of a Boundary Preserving Estimate of Optical Flow, SME Vision Q. 17(3), 1-4, 2001

[6] Gutierrez MA, Rebelo MS, Furuie SS, Meneghetti JC. Automatic quantification of three-dimensional kinetic energy in gated myocardial perfusion single-photon-emission computerized tomography improved by a multiresolution technique. Journal of Electronic Imaging vol. 12(1) 118-124, 2003